Tailoring Rheological Properties of Thermoresponsive Hydrogels through Block Copolymer Adsorption to Cellulose Nanocrystals

Erwan Gicquel, Céline Martin, Quentin Gauthier, Joakim Engström, Clara Abbattista, Anna Carlmark, Emily Cranston, Bruno Jean, Julien Bras

Tailoring rheological properties of thermo-responsive hydrogels through block copolymer adsorption to cellulose nanocrystals

Erwan GICQUEL,[1] Céline MARTIN,[1] Quentin GAUTHIER,[1] Joakim ENGSTRÖM,[2] Clara ABBATTISTA,[1] Anna CARLMARK,[2] Emily D. CRANSTON,[3,4] Bruno JEAN,[5] Julien BRAS[1,6]

[1]Univ. Grenoble Alpes, CNRS, Grenoble INP, LGP2, F-38000 Grenoble, France

[2]KTH Royal Institute of Technology, School of Chemical Science and Engineering, Department of Fiber and Polymer Technology, Teknikringen 56, SE-100 44 Stockholm, Sweden

[3]Department of Chemical and Biological Engineering, University of British Columbia, 2360 East Mall, Vancouver, BC V6T 1Z3, Canada

[4]Department of Wood Science, University of British Columbia, 2424 Main Mall, Vancouver, BC V6T 1Z4, Canada

[5]Univ. Grenoble Alpes, CNRS, CERMAV, 38000 Grenoble, France

[6]Institut Universitaire de France, F-75000 Paris, France

E-mail : julen.bras@lgp2.grenoble-inp.fr

KEYWORDS: Cellulose nanocrystals, PDMAEMA-b-PDEGMA, small-angle neutron scattering, rheology, hydrogel, thermo-responsive, stimuli-responsive, QCM-d, MP-SPR

ABSTRACT

This study investigates the behavior of a thermo-responsive bio-based hydrogel. A block copolymer composed of a quaternized poly(2-(dimethylamino)ethylmethacrylate) (PDMAEMA) cationic polyelectrolyte block and a thermo-responsive block of poly(di(ethylene glycol) methyl ether methacrylate) (PDEGMA) was adsorbed on (2,2,6,6-tetramethylpiperidine-1-oxyl radical) oxidized cellulose nanocrystals (TEMPO-oxidized CNCs or TO-CNCs) to produce hydrogels. PDMEAMA-*b*-PDEGMA was synthesized by atom-transfer radical polymerization and exhibited a lower critical solution temperature between 26 and 28 °C. The extent and dynamics of the adsorption of PDMAEMA-*b*-PDEGMA on TO-CNCs were determined by electromechanical and optical techniques, namely quartz crystal microbalance with dissipation and surface plasmon resonance spectroscopy. Electrostatic adsorption was identified on TO-CNCs with the quaternized block copolymer. Small-angle neutron scattering experiments were performed to investigate the polymer behavior on the TO-CNC surfaces. Depending on the temperature, block copolymer induces the aggregation of nanocrystals after adsorption by connecting CNCs bundles with block copolymer chains. A reversible liquid-to-gel transition, triggered by temperature, was clearly detected by rheological measurements for the copolymer-CNC mixtures at the optimal copolymer to CNC ratio the viscosity increased by four orders of magnitude at low shear rates, due to change in temperatures. These stimuli-responsive functionalities in bio-based hydrogels pave the way for the design of smart CNC-based materials for application in injectable biomedical systems.

Introduction

With the goal to get out of fossil based economy, academic and industrial research has focused on the design of a new generation of materials that are more "bio" (bio-based, bio-compatible, bio-degradable) and "smart" (functional, stimuli-responsive). Nanocelluloses extracted from various cellulose sources have been considered one promising solution. Two major types of nanocellulose exist: cellulose nanofibrils (CNFs) and cellulose nanocrystals (CNCs) [1]. Their differences stem from the isolation methods, dimensions and physical properties. CNFs are flexible filaments of several micrometers long and CNF suspensions present a gel-like behavior at low concentrations due to entangled networks. Oppositely, CNCs are rigid rod-like particles with all dimensions in the nanometer range that form gels only at high concentrations or with additives such as salt, acids, polymers or through surface functionalization with crosslinkable groups [2–4]. Owing to their physical/mechanical properties and high aspect ratio, CNCs, which are generally obtained through acid hydrolysis of cellulose have been suggested for several applications, including environmentally friendly nanocomposites [5–8], biomedical applications [9–15], coatings and printable electronics [16–18], and hydrogels and aerogels [3,6,19].

An important class of functional materials is responsive polymers which are capable of exhibiting changes that can be triggered by external stimuli (pH, temperature, light, redox activity, etc.) [20–23]. The addition of stimuli-responsive functionalities on particle surface can be used to control the release of chemicals from the surface or interactions with other compounds [24], which is promising for biomedical applications, responsive surfaces, and sensors, to name just a few. More specifically, CNC surface modification with thermo-responsive polymers has been shown to significantly enhance the potential applications of CNC systems [2,25–27]. Many approaches to nanocellulose chemical modification have been reported, both covalent and non-covalent [28]. For covalent modification, new properties can be

imparted to CNCs by the modification of hydroxyl groups on their surface. Polymer "grafting onto" and "grafting from" strategies have both been investigated to modify CNCs with responsive polymer chains [23,29–35]. Most of this grafting use complex strategies or toxic compounds which strongly limits upscaling and consequently, their use in biomedical applications. The non-covalent surface modification approach is based on adsorption by ionic, non-ionic, or electrostatic interactions of ions, molecules, or polymers on the surface of CNCs. Only a few studies have investigated the adsorption of stimuli-responsive polymers or monomers on CNCs [36,37]. In some cases, block copolymers have been synthesized with one block being a polyelectrolyte and the other consisting of a thermo-responsive polymer. The polyelectrolyte block will be adsorbed onto surfaces with the opposite charge and the thermo-responsive properties of the other block will be maintained at the surface [33,38–40]. In a recent study by Larsson et al. [39], three block copolymers, containing a thermo-responsive block based on poly(di(ethylene glycol) methyl ether methacrylate) (PDEGMA with a lower critical solution temperature (LCST) tuned between 26 and 28 °C) and a quaternized poly(2-(dimethylamino)ethylmethacrylate) (PDMAEMA) polyelectrolyte block, were synthesized by atom-transfer radical polymerization (ATRP) and then adsorbed onto cellulose nanofibrils in an aqueous suspension. Adsorption at room temperature was investigated by dynamic light scattering (DLS) and quartz crystal microbalance with dissipation monitoring (QCM-d), but no studies on the rheology of such suspensions are available.

The rheological behavior of aqueous CNC suspensions has been studied in detail [41–49]. Shear flow, when applied to nanocrystal suspensions, modifies the liquid microstructure and orientation of the rod-like particles. Above a critical mass concentration, CNC suspensions are shear-thinning, i.e., when the shear rate is increased, the viscosity decreases. Some studies give an explanation on what is happening to the microstructure of CNC suspensions in such cases [41,45].

The expected rheological behavior of systems containing CNCs and thermo-responsive polymers is a reversible liquid form below the LCST (with Newtonian behavior) to a hard hydrogel above the LCST (with a viscosity higher than 100 Pa·s at 1 s^{-1}). This reversible behavior has been investigated in recent scientific studies on drug release [50], stabilization of emulsions [51], gel-entanglement structures [52], and bio-reversible hydrogels [20,53].

In this study, a block copolymer with a PDEGMA thermo-responsive block and a cationic PDMAEMA polyelectrolyte block was synthesized. Based on electrostatic interactions this block polymer could be adsorbed onto TO-CNCs in water suspensions (schematic shown in **Figure 1**). The final system is a thermo-responsive material achieved in aqueous conditions without the need for covalent grafting on the CNC surface. Small-angle neutron scattering (SANS) experiments were performed to understand the block copolymer behavior in the suspension and on the surface of CNCs (mushroom conformation, collapsed chain, etc.). This technique is non-destructive and gives access to the nanoparticle shape, radius of gyration, and specific surface area. Finally, the rheological behavior of the bio-based system was analyzed to understand gel reversibility, which is tuned by the external temperature.

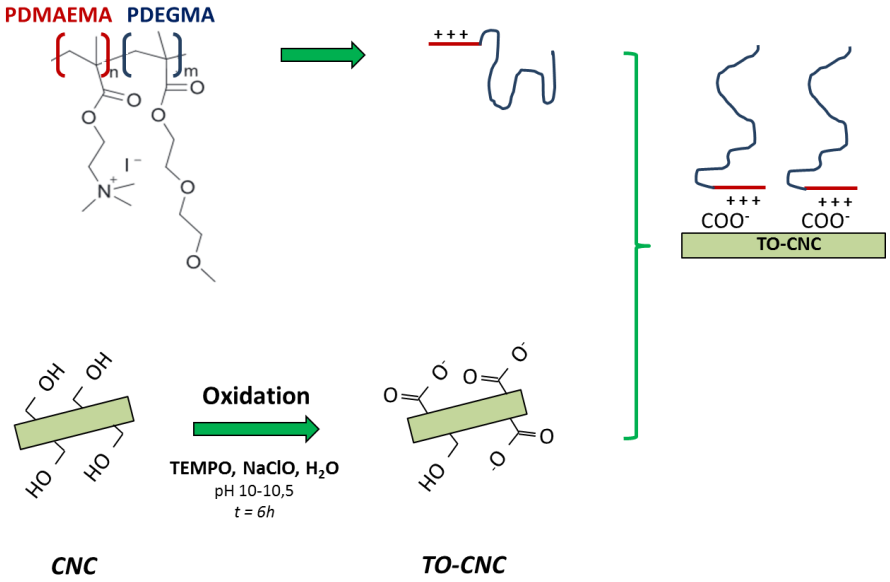

Figure 1. General schematic of diblock adsorption on TEMPO oxidized cellulose nanocrystals

Materials and Methods

Materials

A colloidal suspension of ~12 wt.% commercial cellulose nanocrystals was purchased from the UMaine Development Center (University of Maine, USA). The suspension was produced from wood pulp by sulfuric-acid hydrolysis and was never freeze-dried. The suspension concnentration was measured using a moisture analyzer (Ohaus® MB-35, Sigma Aldrich, USA). For TEMPO oxidation, the following chemicals were purchased from Sigma Aldrich – 2,2,6,6-tetramethyl-1-piperidinyloxy (TEMPO, 2564-83-2), sodium hypochlorite (NaClO, 12 wt.%, 7681-52-9), and sodium bromide (NaBr, 7647-15-6). In addition, ethyl α-bromoisobutyrate (EBiB) (98%), 1,1,4,7,10,10-hexamethyltriethylenetetramine (HMTETA) (97%), copper(I)chloride (99%), and copper(II)chloride (97%) were also procured from Sigma Aldrich. Iodomethane (P99%) was purchased from Riedel-de Haën. Di(ethylene glycol)methyl ether methacrylate (DEGMA) (95%, Aldrich) and 2-(dimethylamino)ethyl methacrylate (DMAEMA) (98%, Aldrich) were activated by passing through a column with neutral and basic aluminum oxides, respectively. Diethyl ether (P99.8%), acetone (100%), dichloromethane (DCM) (P99.8%), tetrahydrofuran (THF) (99.7%), and n-heptane (99.8%) were purchased from VWR. Distilled water was used for all experiments.

Carboxylation of cellulose nanocrystals by TEMPO oxidation

CNCs were subjected to TEMPO oxidation using a previously reported procedure [54]. The CNCs (11 g) were dispersed in 730 mL of distilled water; the resultant suspension was exposed to an ultrasonic dispersive energy of 5 kJ per gram of dry CNCs using a 250-W sonication probe (Sonifier S-250A, Branson, USA) at 50% of the maximum energy. TEMPO (323 mg, 2.07 mmol) and NaBr (3.564 mg, 34.61 mmol) were dissolved in 250 mL of distilled water by magnetic stirring; subsequently, this solution was slowly added to the CNC

suspension. Later, 66 g (0.12 M) of a NaClO suspension was added dropwise to the CNC suspension to start the oxidation reaction. The mixture was stirred for 3 h at room temperature. The pH of the suspension was maintained between 10 and 10.5 by the addition of 0.5 M sodium hydroxide during the reaction, which was later quenched by the addition of ethanol (40 mL); at the end, the color of the suspension turned from yellow to white. The obtained CNCs were washed with 0.5 M HCl to decrease the pH of the suspension to 1–2. The suspension was then centrifuged at least three times (10,000 rpm, 30 min). After the last centrifugation step, the oxidized CNCs were dispersed again in a minimal volume of distilled water to recover all the CNCs. This suspension was then dialyzed against distilled water for at least one week until a neutral pH was obtained (membrane molecular weight cutoff = 6–8 kDa). The obtained TEMPO-oxidized CNCs (TO-CNCs) were stored in a fridge at constant pH to allow the CNCs to exist in their carboxylate form.

Size characterization of CNCs and TEMPO-oxidized CNCs

Transmission Electron Microscopy (TEM): Drops of about 0.001 %wt of CNC suspension were deposited onto glow-discharged carbon-coated TEM grids. After 2 minutes, the excess liquid was absorbed with filter paper, and prior to drying, a drop of Urany-Less (Delta Microscopies, France) was deposited onto the specimen. Then, after 2 minutes, the excess solution was adsorbed with filter paper and the grid was dried at room temperature. The sample was observed using a Philips CM200 (FEI, USA) microscope operating at 200 kV and the most representative images among at least 10 views were selected.

Atomic force microscopy (AFM): Individual nanoparticles of the colloidal suspension were imaged using AFM (Dimension icon®, Bruker, USA). All samples were previously diluted to 10^{-4} %wt and a drop of 0.2 mL was deposited onto freshly cleaved mica plate. Samples are dried overnight under room conditions. Those samples were characterized in tapping mode using a silica coated cantilever (OTESPA® 300 kHz - 42 N/m, Bruker, USA). Scans of 10x10

μm² and 3.3x3.3 μm² were performed to analyze dimensions of CNCs. At least 4 images per samples were obtained. In order to measure length and height dimensions of CNCs, about 200 measurements were performed by using the software ImageJ® to obtain a representative average.

Synthesis of PDMAEMA-b-PDEGMA block copolymers by ATRP

We followed a previously reported method [39] for synthesizing a PDMAEMA macro-initiator and a chain extender with PDEGMA using EBiB as the ATRP initiator together with HMTETA as the ligand and Cu(I)Cl as the halide (initiator:ligand:halide in a 1:2:1 ratio). The synthesis of the macro-initiator, PDMAEMA, was carried out in a 100-mL round-bottomed flask, by first mixing acetone (45 g, target 50 wt.% of monomer), HMTETA (2.08 mL, 7.63 mmol), and EBiB (560.1 μL, 3.82 mmol) by magnetic stirring. The flask was put in an ice bath and DMAEMA (45 g, 286.24 mmol) was added, followed by sealing with a rubber septum, vacuuming for 5 min, and argon filling for 5 min. Before the reaction was activated, Cu(I)Cl (37.8 mg, 3.81 mmol) was added under argon flow to the flask followed by two more vacuum/argon cycles and then immersed in a pre-heated oil bath at 50 °C. The reaction was left to continue for ~1 h with none or low inhibition, targeting 30% conversion (as measured by ^{1}H-nuclear magnetic resonance (NMR)). The reaction was quenched by the addition of 150 mg Cu(II)Cl followed by a cycle of vacuuming and argon to ensure living end-groups. The reaction mixture was passed through a column of neutral aluminum oxide to remove all the copper compounds, followed by two precipitation cycles in cold heptane. The final polymer was left to dry under vacuum overnight and analyzed by ^{1}H-NMR and dimethylformamide (DMF) - size-exclusion chromatography (SEC). Chain extension was carried out according to a previously reported method [39], targeting a DEGMA monomer conversion of around 25% and to achieve a degree of polymerization (DP) of 400 in the PDEGMA block. Typical experiments were carried out by adding PDMAEMA as the macro-initiator (840 mg, 0.134

mmol) in a 50-mL round-bottomed flask, followed by the addition of acetone (40.35 g, target 50 wt.% of the DEGMA monomer). The flask was then immersed in an ice bath. HMTETA (72.87 μL, 0.268 mmol) and DEGMA (40.35 g, 214.4 mmol for reaction DP 1600) were added under argon flow, followed by sealing with a rubber septum and a vacuum/argon cycle. Similar to the macro-initiator synthesis, the chain extension reaction was activated by the addition of Cu(I)Cl (13.26 mg, 0.134 mmol) and run at 50 °C in an oil bath after two vacuum/argon cycles. The resulting polymer was terminated by letting in air and purified by precipitating twice with cold heptane. The final block copolymer was analyzed by ^{1}H-NMR and DMF-SEC. Typical experiments for quaternization of the block copolymer, PDMAEMA-*b*-PDEGMA, were performed in a beaker according to a previously reported method [39]. The use of iodomethane yields a three times excess stoichiometric amount to DMAEMA units (ca DP25). Iodomethane was pre-dissolved in 15 mL of THF and added dropwise to a beaker with PDMAEMA-*b*-PDEGMA (2 g) in THF (25 mL) and left overnight to react under vigorous stirring and precipitated in cold heptane; this mixture was then re-dissolved in water and precipitated in cold acetone, followed by final isolation via freeze-drying. In this study, the block copolymer will also be called diblock (DB).

Characterization of the PDMAEMA-*b*-PDEGMA block copolymer

^{1}H-NMR spectra were recorded at room temperature on a Bruker Avance 400 MHz spectrometer, using $CDCl_3$ and D_2O as the solvents. ^{1}H-NMR was used to analyze both the polymerization kinetics and monomer conversion to polymer and to estimate the degree of quaternization of DMAEMA units in the block copolymer. SEC was performed using DMF (0.2 mL min^{-1}) as the mobile phase at 50 °C on a TOSOH EcoSEC HLC-8320GPC system equipped with an EcoSEC RI detector and three columns (PSS PFG 5 lm; Microguard, 100 Å, and 300 Å) (MW resolving range: 300–100,000 Da) from PSS GmbH. The molecular weight (M_n and M_w) and the polymolecularity index ($Đ_N$) were calculated using a conventional

calibration method with linear poly(methyl methacrylate) (PMMA) as the standard. Corrections for flow-rate fluctuations were made using toluene as an internal standard. PSS WinGPC Unity software version 7.2 was used to process the obtained data.

Polyelectrolyte titration (PET) was carried out to measure the charge density of the block copolymers using a 716 DMS Titrino from Metrohm (Switzerland). Potassium polyvinyl sulfate (KPVS) was used as the titrant and orthotoluidine blue (OTB) was used as the indicator. The color change was recorded with a fotoelektrischer Messkopf 2000 from BASF and the amount of KPVS needed to reach the equilibrium point was calculated according to the method developed by Horn[55].

PDMAEMA-*b*-PDEGMA adsorption onto TEMPO-oxidized CNCs in suspension

Adsorption of the PDMAEMA-*b*-PDEGMA block copolymer onto TO-CNCs in suspension was carried out at 15 °C, a temperature below the LCST of the block copolymer (24 °C). The freeze-dried block co-polymer was directly added to the suspension of CNCs at different weight percent concentrations and dispersed by stirring with a magnetic stir bar over 4 h.

Adsorption experiments using quartz crystals microbalance with dissipation (QCM-d)

Cellulose model surfaces were prepared on quartz crystal sensors coated with gold (QSX 301), supplied by Biolin Scientific AB (Sweden) to determine the amount of copolymer adsorbed onto CNCs using QCM-d. QCM-d sensors were first washed with a piranha cleaning solution (H_2O_2 mixed with H_2SO_4 at a 1:3 ratio) for 20 min, rinsed with distilled water, and dried with N_2. Next, the sensor was spin-coated with a 0.1 mM suspension of polyethyleneimine (PEI, Sigma Aldrich, 750 000 $g \cdot mol^{-1}$) at 4000 rpm for 30 s (SPIN150i Tabletop, spin coating POLOS, The Netherlands) and rinsed with deionized water to remove any unbound polymer from the surface. Finally, the colloidal suspension of TO-CNCs (1

wt.%) was spin-coated on top of the PEI layer and rinsed using the same protocol. The films were heat treated at 80 °C in the oven overnight to ensure stability in aqueous media. The surface coverage of CNCs after spin coating was evaluated by AFM measurements [56].

The interaction between TO-CNC films and the block copolymer was then measured using QCM-d (E1 model, Biolin Scientific Holding AB, Gothenburg, Sweden). The CNC-coated sensors were mounted in the QCM-d chamber and exposed to a flow of MilliQ water to create a stable baseline before block copolymer injection (2 h). All the experiments were conducted at a constant temperature of 18 °C. The block copolymer was injected at a flow rate of 17 mL/h at a concentration of 1 mM (based on polymer molecular weight). After reaching a plateau in adsorption, rinsing was carried out with a flow of MilliQ water.

The principles of QCM-d have been described previously by Rodahl et al. [57]. Changes in the sensor's resonance frequency are related to the mass adsorbed or desorbed to the sensor. The QTools software (version 3.0.15, Biolin) was used for analysis of the frequency and dissipation data (for overtones 3, 5, 7, 9, 11, and 13). The estimated adsorbed copolymer amount (Δm) was calculated using the Sauerbrey equation (**Equation 2**) [58] with an assumption that the adsorbed copolymer film is rigid.

$$\Delta m = -C\frac{\Delta f}{n} \qquad (2)$$

Where, C is a constant related to the density and thickness of the quartz crystal sensor and it has a value of 17.7 ng·cm^{-2}·Hz^{-1} for a 5 MHz sensors (provided by the manufacturer), Δf is the change in frequency, and n is the overtone number. In this study, the third overtone was used for calculating Δm.

The Sauerbrey model is generally assumed to be valid if the dissipation change is less than 10 times the change in frequency change [59,60], if the coating is uniform and continuous on the sensor and if the coated mass is small compared to the mass of the sensor [33]. Furthermore,

many studies have shown that there is only a small difference between the Sauerbrey and more advanced viscoelastic models, such as the Voigt model [61–63].

Adsorption experiments using multi-parametric surface plasmon resonance spectroscopy (MP-SPR)

Cellulose model surfaces were prepared on MP-SPR gold sensors coated with SiO_2 (SPR102-SiO_2), supplied by BioNavis (Finland) to determine the amount of block copolymer adsorbed onto CNCs using MP-SPR. MP-SPR sensors were first washed using a piranha cleaning solution as described above for QCM-d sensors. Next, the sensor was spin-coated with a 2 wt.% suspension of TO-CNCs at 4000 rpm for 30 s (G3P Spincoat, Specialty Coating Systems Inc. Indianapolis, USA). The films were heat treated at 80 °C in the oven overnight to ensure stability in aqueous media. Sensors were then rinsed with deionized water to remove any unbound CNCs from the surface and heat-treated again at 80 °C for 2 h. The full surface coverage of MP-SPR sensors was verified by AFM.

Block copolymer adsorption onto TO-CNCs was monitored in real time using MP-SPR (Navi 200, BioNavis, Ylöjärvi, Finland) and "full-angular scan" curves (40°–77°) were collected. TEMPO CNCs films were swollen under a constant MilliQ water flow of 100 $\mu L \cdot min^{-1}$ at 18 °C for 1 h for equilibration (more details can be found in the work of Reid et al [64]) followed by block copolymer injection at 100 $\mu L \cdot min^{-1}$ at a concentration of 0.5 mM.

Detailed information on the MP-SPR optical and flow systems are presented in the study by Liang et al. [65]. The MP-SPR instrument measures changes in the refractive index near the sensor surface as follows: a laser beam is reflected off the back surface of the sensor through a prism. Above a given angle (angle of total internal reflection) an evanescent wave is "leaked" into the sensor's metal generating surface plasmons. At the angle where the laser beam energy and momentum match those of the plasmons a sharp dip in the reflected laser intensity is

measured (called the SPR "peak"). When changes occur at the sensor surface, such as adsorption/desorption or film swelling, the SPR peak angular position shifts [66]. The instrument used in this work has two lasers with wavelengths of 785 and 670 nm (hence "multiparametric") with a spot size of 500 × 500 μm^2, however, due to significant copolymer adsorption, only the 785 nm laser data was within the measureable angular range.

Equation 3 was used to determine the thickness (d) of the adsorbed layer in nanometers from MP-SPR [67].

$$d = \frac{l_d}{2} \times \frac{\Delta SPR_{angle}}{m(n_a - n_0)} \quad (3)$$

Here, ΔSPR_{angle} is the change in SPR peak angle during adsorption, l_d is the characteristic evanescent electromagnetic-field decay length, which is estimated to be 0.37 times the wavelength (785 nm), m is the sensor sensitivity factor (81.015°), and n_0 and n_a are the refractive indices of the bulk solution (1.334) and adsorbed substance, respectively. n_a was estimated to be 1.46 for the block copolymer (based on POEGMA) [68]. Later, the amount of adsorbed polymer per unit area was calculated using **Equation 4** [69].

$$\Delta m = d \times \rho \quad (4)$$

Here, d is the thickness of the adsorbed layer and ρ is the packing density of the adsorbed copolymer. According to the results of Feng et al. [70], the value of ρ was taken to be 1.12 g·cm^{-3}.

Small-angle neutron scattering: Polymer behavior after adsorption

In order to investigate polymer behavior on the surfaces of CNCs after block copolymer adsorption, SANS experiments were performed. The concentrations of the different suspensions were as follows: 1 wt.% for TO-CNCs, 1 wt.% for the block copolymer, and 1 wt.% of the block copolymer adsorbed on 1 wt.% TO-CNCs. As SANS is sensitive to isotopic composition, all the samples were dialyzed against D_2O in order to obtain the best contrast

possible and to minimize incoherent scattering due to hydrogen. SANS experiments were carried out using a PA20 spectrometer at le Laboratoire Léon Brillouin (CEA, Saclay, France). A large range of the scattering vector, Q, between 0.0024 and 0.044 $Å^{-1}$ was probed using three different neutron wavelength/sample-detector distances (5 Å/18 m, 5 Å/8 m, and 5 Å/1.5 m). The samples were studied at 20 °C and 40 °C, i.e., below and above the polymer LCST, respectively. The samples were loaded in quartz cells (Hellma) with a path length of 2 mm. The averaged spectra were corrected for the solvent (D_2O), cell, and incoherent scattering (cell with 1 mm of H_2O), as well as the background noise [71] and spectra $I(Q) = f(Q)$ on an absolute scale. The data were fitted using the SasView® 4.0.1 modeling software.

Rheological experiments on the thermo-reversible hydrogels

The rheological behavior of hydrogels under shear stress was studied using a rotational rheometer (Physica MCR 301 and MCR 302, Anton Paar, Austria). To investigate the temperature effect and reversibility of these systems, tests were carried out below the LCST (15 °C) and above the LCST (40 °C). Start-up shearing tests were performed with a cone-plate configuration (diameter of 50 mm and angle of 1°). The atmosphere around the sample was saturated with water to avoid evaporation during measurement.

To control the initial state of each sample, a constant shear rate was applied (10 s^{-1} for 30 s). The transient response under shear was recorded until steady conditions were obtained. Steady-shear viscosity versus shear-rate curves were generated for each sample in the shear rate range of 0.01 to 1000 s^{-1}. The time required to reach steady conditions decreased with an increase in the shear rate.

Results and Discussion

Hydrogel material characterization

TEMPO oxidation of cellulose nanocrystals

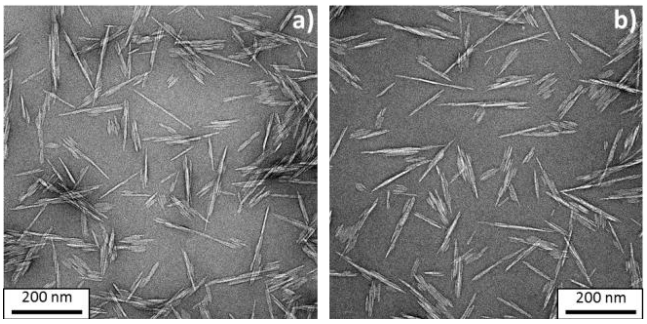

Figure 2. TEM images of a) CNCs and b) TO-CNCs.

After extraction from wood pulp with sulfuric acid, CNCs exhibit a rod-like shape, as shown in **Figure 2a**. Size measurements on TEM images show an average length of 150 ± 30 nm and a cross-section of 10 ± 5 nm. These values are comparable with those reported previously [72]. Oxidizing the CNCs through TEMPO-mediated oxidation did not change their size or appearance (**Figure 2b**). The sulfate half-ester content on CNCs was 200 μmol·g^{-1} and the carboxylate content after oxidation was found to be 1450 μmol·g^{-1} which corresponds to a degree of oxidation of 0.25 mol/mol of anhydroglucose unit, determined by conductometric titration (see ***Supporting Information - Figure S1***).

Synthesis of the PDMAEMA-b-PDEGMA block copolymer by ATRP

The PDMAEMA-*b*-PDEGMA block copolymer was successfully synthesized using Cu(I)-mediated ATRP. It results in a relatively narrow macro-initiator followed by a successful chain-extension reaction, as can be judged by the SEC results in **Table 1**. The charge density is only present on block of PDMAEMA. The molecular weight of the responsive block is much higher than the polyelectrolyte block in order to favor stimuli-responsive properties. As previously described by Vuoriluoto et al. [33] and Larsson et al. [39], the anchoring first block of

PDMAEMA contains tertiary amine groups which are quaternized (permanent cationic charges) by methylation.

Table 1. Data corresponding to the polymerization of the PDMAEMA-b-PDEGMA block copolymer

Sample	M_n[a] [g/mol]	M_n[b] ($Đ_N$) [g/mol]	Charge density [meq/g][c]
PDMAEMA macro-initiator	3 700	7 060 (1.20)	3.065
PDMAEMA-*b*-PDEGMA	39 000	119 700 (1.21)	0.340

[a] Calculated from ^{1}H-NMR conversion 30% of PDMAEMA and 25% of DEGMA block. [b] From analysis in DMF-SEC. [c] Measured by PET

Adsorption of PDMAEMA-*b*-PDEGMA to TO-CNC Films

Figure 3 presents the adsorption results for the PDMAEMA-b-PDEGMA block copolymer and TO-CNC films measured by QCM-d (**Figure 3a**) and MP-SPR (**Figure 3b**). These experiments probe the copolymer-CNC interactions in two-dimensions and will later be compared to adsorption in suspension (i.e., in three-dimensions). Strong copolymer adsorption was measured by both techniques and is attributed to electrostatic attraction between anionic CNCs and the cationic block of the copolymer (PDMAEMA). The fast adsorption (that reaches a plateau within minutes) and no removal of copolymer upon rinsing is typical behavior for adsorption driven by electrostatic interactions [73]. Based on previous work with grafting and adsorption of polyethylene glycol (PEG) and PEG-based polymers onto CNCs, no adsorption to cellulose is expected from the PDEGMA block [74–76].

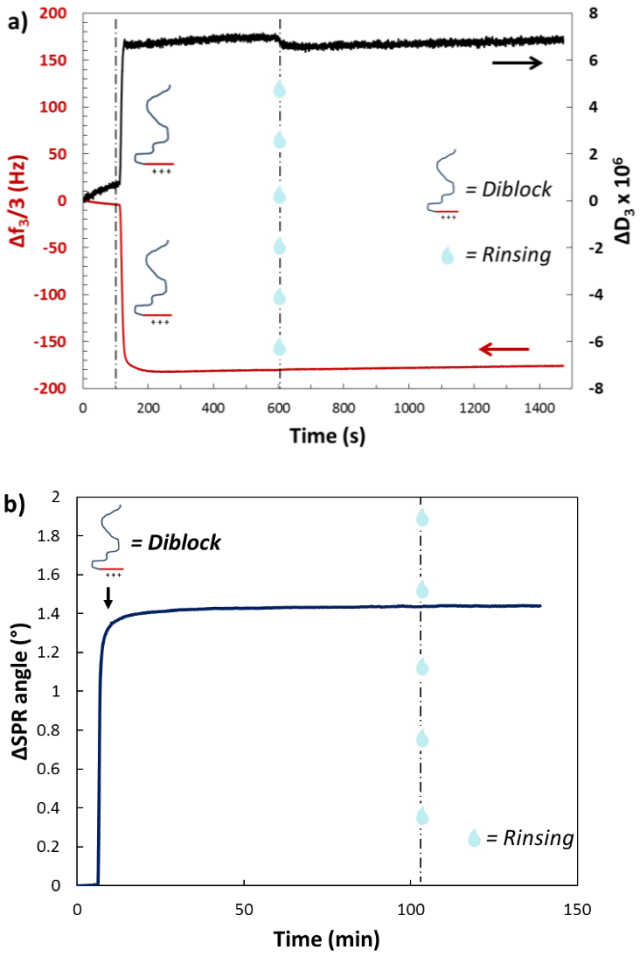

Figure 3. Adsorption of PDMAEMA-b-PDEGMA copolymer onto TO-CNC films. a) QCM-d results where the adsorption was measured at 15°C, pH 5.5, flow rate at 300 µL/min and copolymer concentration of 1 mM. The block copolymer was injected at 100 seconds (pH = 5.4) and the rising with MilliQ water started at 600 seconds. Δf_3 (left axis) and ΔD_3 (right axis) are the shift in frequency and dissipation for overtone 3, respectively. b) MP-SPR results where adsorption was carried out at 18°C, pH 6, flow rate of 100 µL/min, and copolymer concentration of 0.5 mM. The block copolymer was injected at 6 min and the rising with MilliQ water started at 105 min.

Table 2 summarizes the adsorbed amounts of the block copolymer on TO-CNC films from QCM-d and MP-SPR measurements; the values are very similar at 30 and 23 $mg \cdot m^{-2}$, respectively. This large adsorbed mass is due to the high surface charge density of carboxylated TO-CNCs (at pH 5.5) and the high molecular weight of the block copolymer.

The small discrepancy between techniques can be attributed to the mass of water coupled to the copolymer, which is detected by QCM-d but not by SPR. The strong adsorption of PDMAEMA-*b*-PDEGMA to cellulose and the adsorbed amounts agree with previous studies showing similar block copolymer adsorption to CNF films [33] and TEMPO-oxidized CNF films [33,38,39]. In the MP-SPR results of Vuoriluoto [33], the amount of block copolymer (D_{33}-$EGMA_{137}$) adsorbed on TEMPO CNF were 6.1 $mg \cdot m^{-2}$ which is lower than the present 20 $mg \cdot m^{-2}$ for D_{29}-$EGMA_{180}$. After spin coating on sensors, CNC exhibit a higher film density than CNF, which corresponds to a higher amount of negative charge and also to a higher amount of block copolymer adsorbed on CNC coated sensor.

Table 2. Block copolymer adsorption to films - 2D experiments: QCM-d results present frequency and dissipation changes and adsorbed mass, Δm, (**Equation 2**) from PDMAEMA-b-PDEGMA adsorption to TO-CNC films. MP-SPR results show the layer thickness, d, (**Equation 3**) and adsorbed mass (**Equation 4**) from PDMAEMA-b-PDEGMA adsorption to TO-CNC films.

	QCM-d			**MP-SPR**	
Surface	$\Delta f_3/3$ (Hz)	ΔD_3 (10^6)	Δm ($mg \cdot m^{-2}$)	d (nm)	Δm ($mg \cdot m^{-2}$)
TO-CNCs	-175.8	6.9	30.0 ± 0.1	20.5	23.0 ± 0.4

Structural investigation by SANS

SANS measurements were performed to obtain structural information on both the individual components, namely TEMPO-oxidized CNCs and PDMAEMA-b-PDEGMA block copolymer, and on a sample composed of a mixture of TO-CNCs and block copolymers with a 1:1 TO-CNC:DB mass ratio.

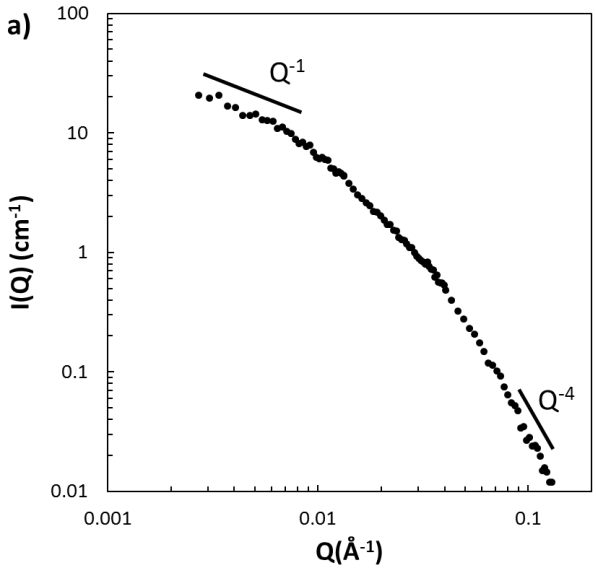
a)
100
10
1
0.1
0.01
I(Q) (cm-1)
Q-1
Q-4
0.001
0.01
0.1
Q(Å-1)

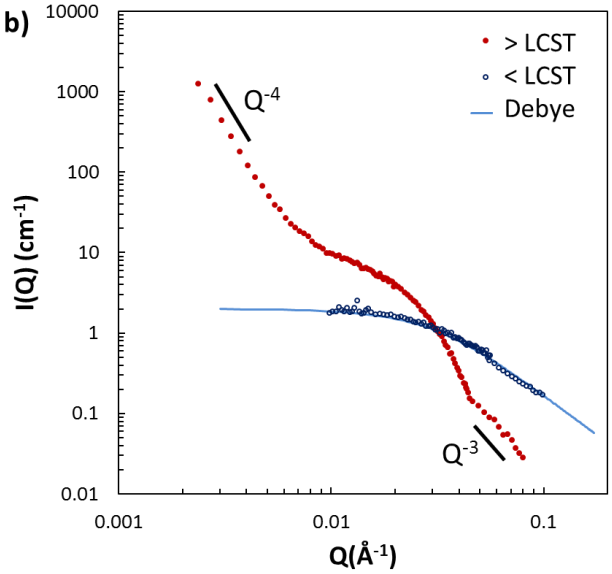
b)
10000
1000
100
10
1
0.1
0.01
I(Q) (cm-1)
> LCST
< LCST
Debye
Q-4
Q-3
0.001
0.01
0.1
Q(Å-1)

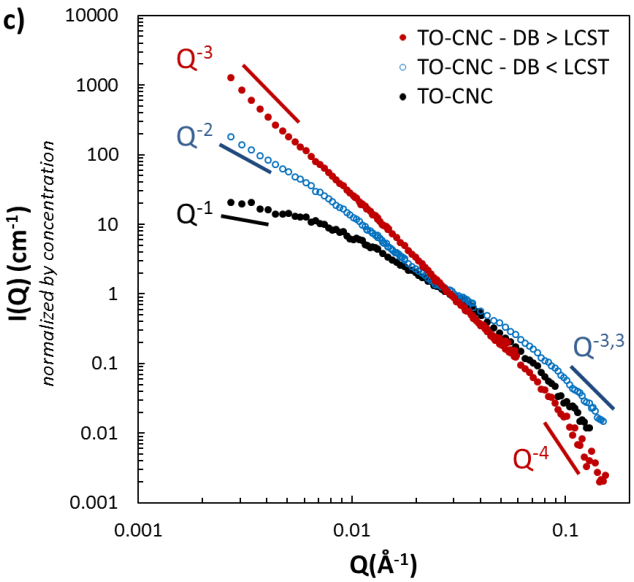
c)
10000
1000
100
10
1
0.1
0.01
0.001
I(Q) (cm-1)
normalized by concentration
TO-CNC - DB > LCST
TO-CNC - DB < LCST
TO-CNC
Q-3
Q-2
Q-1
Q-3,3
Q-4
0.001
0.01
0.1
Q(Å-1)

Figure 4. SANS curves for a) TO-CNCs at 20°C, b) PDMAEMA-b-PDEGMA block copolymer (DB) below and above the LCST and c) TO-CNCs (black dot), TO-CNCs mixed with block copolymer system under (blue open circle) and above the LCST (red dot). I(Q) was normalized by the suspension concentration. Slope fitting curves are indicated on each graph. The concentrations of the different suspensions/solutions were as follows: 1 wt.% for TEMPO CNCs, 1 wt.% for the block copolymer, and 1 wt.% of the block copolymer adsorbed on 1 wt.% TEMPO CNCs

Figure 4a shows the SANS spectrum of a 1 wt.% TO-CNCs suspension in D_2O. In the low Q-region, the intensity decays as Q^{-1}, which is the characteristic decay of rod-shaped objects. In the high-Q region, a Q^{-4} decay is observed, which reflects a sharp and smooth interface between the particles and the solvent. These features, which are the same as those reported for as-prepared (*i.e.* non-oxidized) CNCs [77], show that the TEMPO oxidation does not significantly affect the morphology of TO-CNCs, which consist of rod-like objects with a smooth surface. A quantitative analysis was further performed by fitting the TO-CNC spectrum in **Figure 1** using the form factor of parallelepipedic particles. Such an analysis could be carried out due to the dilute conditions used, which allowed us to consider the sample as being composed of non-interacting particles and therefore to neglect the influence of the structure factor. As shown in **Supporting Information Figure S2**, a good fit of the data could be obtained, giving average dimensions of 150 nm × 19 nm × 4 nm. The accuracy on the length value is low, due to the lack of data in the very low-Q-range, but these dimensions are in good agreement with previously reported values. Furthermore, a good agreement with dimensions extracted from a statistical analysis of the TEM images is also obtained.

Figure 4b shows the SANS spectra of 1 wt.% DB solutions at 20 °C and 40 °C, *i.e.*, below and above the polymer's LCST, respectively. Below the LCST, the DB signal in the probed Q-range corresponds to a low-Q plateau followed by a Q^{-2} decay, showing that the absence of

aggregates and that DB chains obey Gaussian statistics. The spectrum could be fitted using the Debye function that characterizes polymer chains in theta solvent [78] and the radius of gyration of the DB extracted from this analysis is about 4.8 nm. This value is fairly consistent with what is expected from ~40000 g/mol polymers.

The dimensions extracted from the SANS measurements for both the TO-CNC and the DB were used to estimate the DB to CNC ratio that corresponds to full coverage of the CNC surface by DB chains. In this estimation, surface saturation is defined as the point where all the available CNC surface is covered with non-overlapping adsorbed DB coils with the tighter possible packing, which corresponds to 90% of the CNC surface in the case of a hexagonal packing. Using the aforementioned dimensions for TO-CNCs and of Rg~4.8 nm for the DB coils, it can be estimated that the surface saturation of a TO-CNC is reached when about 80 DB chains are adsorbed. This value corresponds to a TO-CNC/DB mass ratio of 3.

As expected, a different SANS spectrum is obtained for the block copolymer solution when the temperature is increased above the LCST. The intensity decays as Q^{-4} in the low Q-region, which can be attributed to the formation of dense and large-size aggregates formed by the association of collapsed chains in these bad solvent conditions. In the intermediate Q-region the intensity decay is somehow similar to the form factor of polydisperse spheres but no attempts to precisely fit these data with a model was performed. The Q^{-3} decay in the high Q-region indicates the rough character of these rather well-defined globules.

Figure 4c shows the SANS result for a system based on TO-CNCs and block copolymers in a 1/1 mass ratio, below and above the LCST of the DB. Below the LCST, the Q^{-2} dependence and the very significant increase in the scattering intensity (when compared to TO-CNCs) in the low Q-region is not compatible with rod-shaped particles anymore but rather corresponds to the presence of CNC bundles, possibly connected by DB chains. The high slope in the high Q-region (between Q^{-3} and Q^{-4}) is not compatible with the adsorption of polymer chains that should give a Q^{-2} decay for adsorbed swollen coils (mushroom regime) or Q^{-1} decay for

adsorbed extended polymer chains (brush regime). SANS data therefore show that the sample is not composed of individual CNCs decorated by adsorbed DB chains on their surface but rather prove that the polymer induces the aggregation of CNCs. This result is in line with dynamic light scattering data yielding high hydrodynamic diameters values (data not shown) and is possibly a result of the large excess of DB chains in this samples when compared to the estimated saturation. Heating such a sample at a temperature higher than the LCST has strong consequences on the SANS spectrum that exhibits a close to Q^{-3} decay on a very extended Q-range, showing the formation of dense aggregates at all probed length scales.

Rheological behavior of the hydrogels

Rheological behavior of TO-CNCs and block copolymers

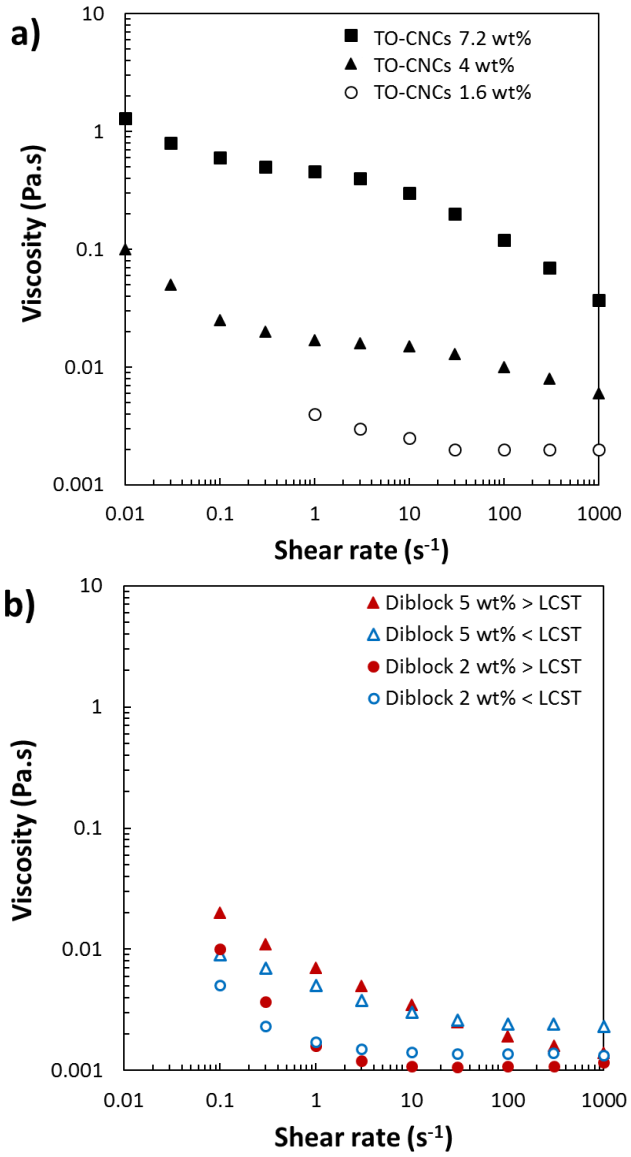

Figure 6. Flow curves of a) TO- CNCs at 1.6, 4 and 7.2 w.t% at 20°C and b) diblock at 2 and 5 wt.% below (15°C) and above (40°C) its LCST.

Figure 6 shows the flow curves of different raw materials used in this study. The rheological behavior of TO-CNCs (**Figure 6a**) is analyzed at different concentrations. The rheological behavior of dilute suspensions is similar to that of a Newtonian fluid. When the concentration increases, this behavior shifts to that of a shear-thinning fluid and a three-slope behavior appears at higher shear rates. This behavior is characteristic of a chiral nematic phase for non-

oxidized CNCs [45,47,79]. **Figure 6b** shows the rheological behavior of the block copolymer at different concentrations and temperatures (above and below the LCST of the thermo-responsive polymer). The PDEGMA block is thermo-responsive as described earlier [39]. Whatever the concentration is (up to 5 wt.%), the viscosity is never greater than 0.2 Pa·s at a shear rate of 0.1 s^{-1}. Further, there was no clear difference in its viscosity at the LCST. The constant behavior between these two temperatures is probably because the polymer does not exhibit any entanglement at this concentration when the LCST is reached. Below the LCST, the block copolymer exists in the form of a random coil and does not resist shear. Above the LCST, it precipitates. Nevertheless, in the absence of anchorage, the collapsed globules of the diblock flow under the action of a shear rate.

Influence of TO-CNCs on the rheological behavior of the block copolymer solution

The rheological behavior of TO-CNCs/DB mixtures was first investigated at a constant block copolymer concentration of 3 wt.% and varying TO-CNCs:block copolymer mass ratios, namely 2:1 (**Figure 7a**), 1:1 (**Figure 7b**), and 0.5:1 (**Figure 7c**). As shown by QCM-D and MP-SPR data, DB chains strongly adsorb onto TO-CNCs but according to the surface saturation estimated from a geometrical approach and using SANS data, each of these ratios corresponds to bulk samples where the DB is in excess, *i.e.* a fraction of the DB chains is adsorbed on the CNCs and another fraction consists of free chains in solution. At low shear rates (< 0.1 s^{-1}), the viscosity of both individual TO-CNCs (**Figure 6a**) suspensions and individual block copolymers solutions (**Figure 6b**) is low and below 1 Pa·s, whatever the concentration value in the range probed. However, in the case of mixtures of the two species for TO-CNC:DB mass ratios equal to 2:1 and 1:1, viscosity values as high as 100 Pa·s were measured (**Figure 7a** and **7b**). For these two samples, when the shear rate is increased, a shear-thinning behavior can be observed with a viscosity decrease down to 0.1 Pa·s for a shear rate of 100 s^{-1}. In both these cases, a significant synergistic effect is thus observed below the LCST. However, increasing the temperature above the LCST has little effect on the

viscosity, showing that under these conditions the system does not exhibit any temperature-sensitive behavior despite the presence of the thermosensitive DB. These results are consistent with samples being composed of polymer-mediated aggregated CNCs, as revealed by SANS for the TO-CNC:DB 1:1 sample. It can be assumed that within these mixed bundles most of the block copolymer chains are involved in the creation of bonds with and between the CNCs, which suppresses their thermosensitive character. High shear rates presumably induce a weakening of interactions between aggregates or a reduction of their size, which results in low viscosity values since, as the shear rate increases, the system would more and more behaves as a mixture of individualized particles.

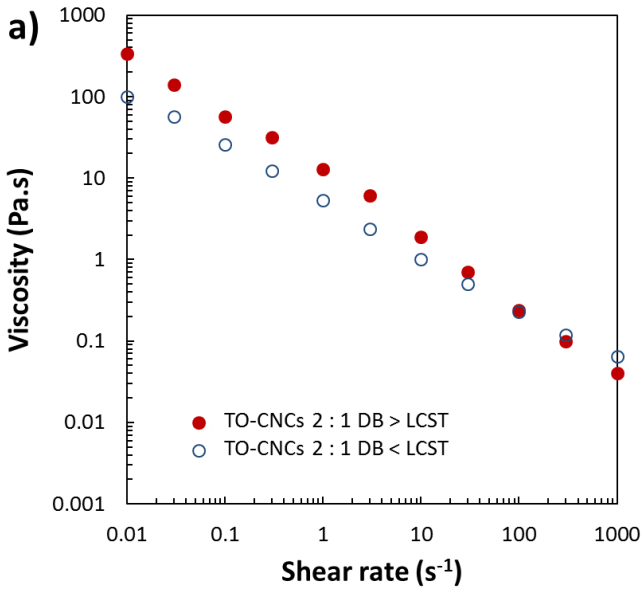
a)
Viscosity (Pa.s)
1000
100
10
1
0.1
0.01
0.001
0.01
0.1
1
10
100
1000
Shear rate (s-1)
TO-CNCs 2 : 1 DB > LCST
TO-CNCs 2 : 1 DB < LCST

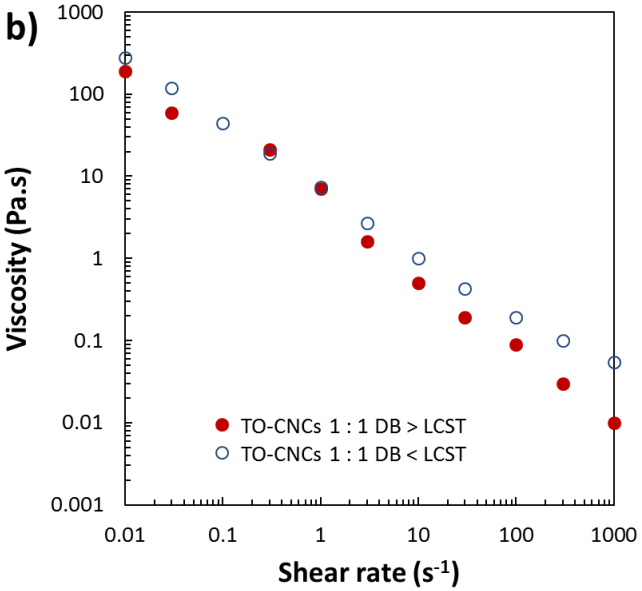
b)
Viscosity (Pa.s)
1000
100
10
1
0.1
0.01
0.001
0.01
0.1
1
10
100
1000
Shear rate (s-1)
TO-CNCs 1 : 1 DB > LCST
TO-CNCs 1 : 1 DB < LCST

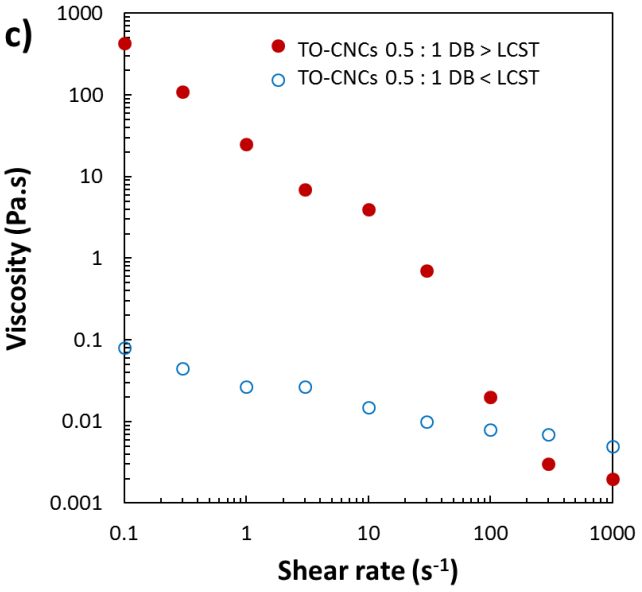
c)
Viscosity (Pa.s)
1000
100
10
1
0.1
0.01
0.001
0.1
1
10
100
1000
Shear rate (s-1)
TO-CNCs 0.5 : 1 DB > LCST
TO-CNCs 0.5 : 1 DB < LCST

Figure 7. Flow curves under (ring) and upper (dot) the LCST of a 3 wt.% diblock solution with a) 6 wt.% TO-CNCs (ratio 2:1), b) 3 wt.% TO-CNCs (ratio 1:1) and c) 1.5 wt.% TO-CNCs (ratio 0.5:1).

The rheological behavior shown in **Figure 7c** for a TO-CNC:DB 0.5:1 mass ratio is completely different. Indeed, below the LCST, for this more limited amount of TO-CNC in the sample, there was no clear synergistic effect and the sample exhibits a low viscosity similar to the one obtained for a pure TO-CNCs suspension. Nonetheless, when the temperature is increased above the LCST of the DB, a considerable thermal transition is observed with an increase in the viscosity by more than three decades at a low shear rate (0.1 to 400 Pa·s at 0.1 s^{-1}). At higher shear rates (>10 s^{-1}), the viscosity drastically decreased to reach low values below 0.01 Pa·s above 300 s^{-1}. It can be assumed that at this lower TO-CNC content the size of the CNC aggregates is smaller than for higher TO-CNC:DB ratio and that the system tends to comprise individual CNCs particles with adsorbed block copolymer chains. Block copolymer chains in excess are not involved in connecting CNCs and these chains retain their thermo-responsive behavior. As a consequence, the sample behaves below the LCST like a polymer-decorated TO-CNC suspension, with a viscosity slightly higher than a pure TO-CNC sample. Above the LCST the thermo-responsive block collapses and becomes hydrophobic, which leads to CNC aggregation and cross-linking, resulting in a high increase in viscosity. Such a situation is reminiscent of the case of thermo-responsive polymer-grafted CNCs reported by Hemraz et al. and Azzam et al. [20,53].

Influence of the TO-CNC and block copolymer ratio on the rheological behavior of the hydrogels

In the second part of the rheology study, the final concentration of the suspension was fixed at 5 wt.% and the influence of the ratio between TO-CNCs and block copolymer on the rheological behavior of the hydrogels was evaluated (**Figure 8**). As suggested by the QCM-D

results (**Figure 3a**) and MP-SPR measurements (**Figure 3b**), the block copolymer exhibits a high tendency to adsorb irreversibly on TO-CNCs. Four ratios TO-CNCs:DB were selected: 2:1, 1:1, 1:2, 1:4.

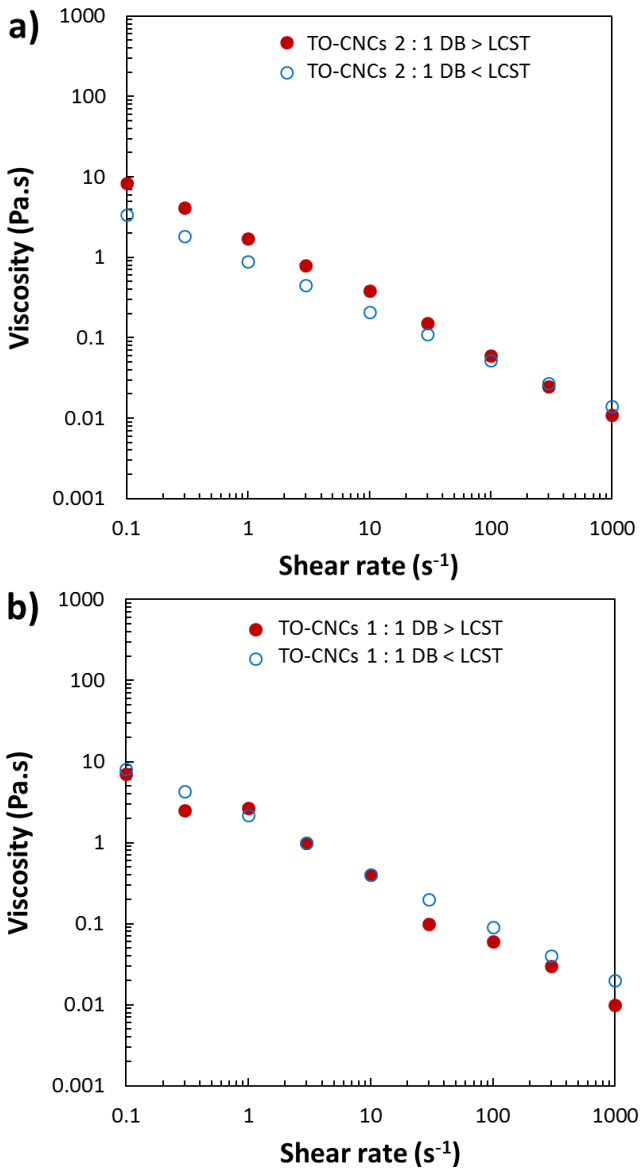

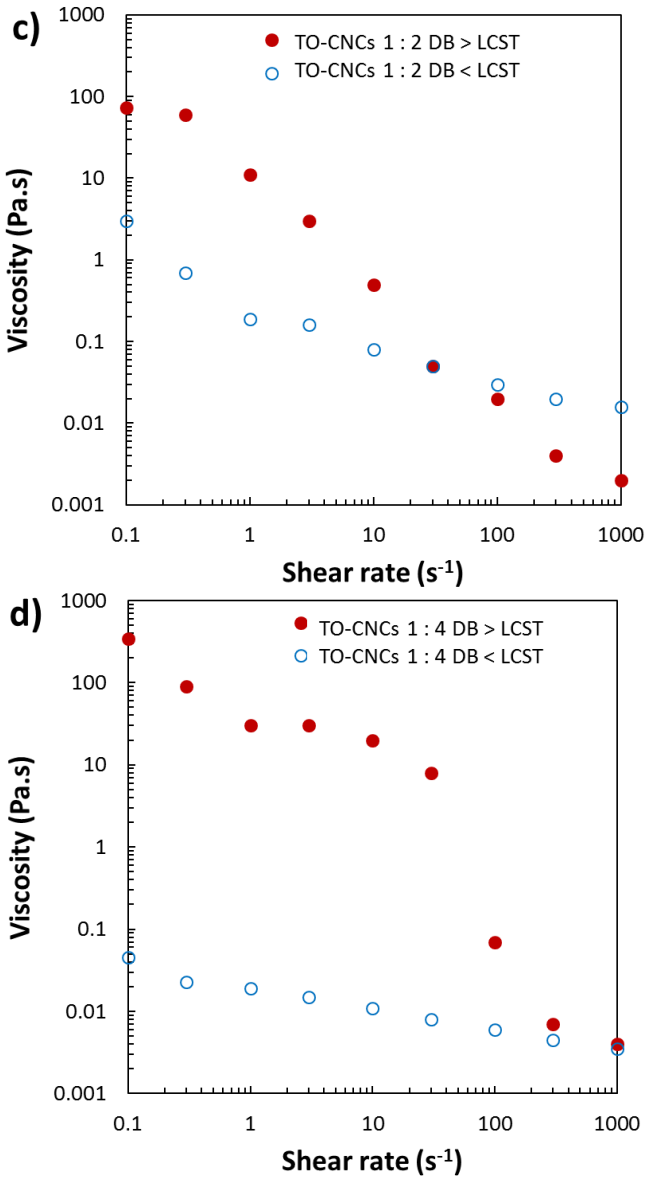

Figure 8. Flow curves (ring) and upper (dot) the LCST for final system concentration of 5 wt% with different ratio of TO-CNCs for diblock of a) 2:1, b) 1:1, c) 1:2 and d) 1:4.

For the first two ratio values, as shown in **Figures 8a** and **8b**, the rheological behavior of the mixed suspension below the LCST exhibits a significant synergistic effect when compared to pure DB solutions or pure TO-CNC suspensions. However, in both cases, increasing the temperature above the LCST had no significant effect on the rheological behavior, i.e. both systems are not thermo-responsive. The viscosity is lower than the viscosity measured in **Figures 7a and 7b** (10 against 200 Pa·s) due to a suspension concentration divided by two for the present samples, which influences the rheological behavior of the hydrogel.

In **Figure 8c** the TO-CNCs:DB 1:2 (in a consistent manner with the ratio 0.5:1 on **Figure 7c**), the amount of block copolymer with respect to the TO-CNCs increases and seems to create a thermo-responsive system. Below the LCST, the flow curve indicates a similar viscosity on the all shear rate range than TO-CNCs:DB 2:1 (**Figures 8a**) and 1:1 (**Figure 8b**). Besides, above the LCST, the viscosity increases at a low shear rate (<1 s^{-1}). The block copolymer amount is sufficient to allow the existence of CNCs as individual particles with some adsorbed chains and its thermal responsivity in the suspension. At higher shear rates (>3 s^{-1}), the system's structure is broken due to shear. At shear rates greater than 100 s^{-1}, the viscosity reduces to below 0.01 Pa·s because of the expulsion of aggregates out of the suspension by centrifugation (visual observation after rheological experiments).

The system with TO-CNCs:DB 1:4 (**Figure 8d**) exhibits a very promising thermo-responsive result when the block copolymer is present in a large amount as compared to TO-CNCs. Below the LCST, no clear synergistic effect is visible and the system exhibits low viscosities (<0.1 Pa·s). However, above the LCST, the system displays an impressive thermo-responsive behavior. At a shear rate of 0.1 s^{-1}, the viscosity increases by about 760 times when the LCST is reached (340 Pa·s). Up to 30 s^{-1}, the viscosity follows a plateau trend. It overcomes the resistance of adsorbed systems to flow, probably due to the network of the thermo-responsive polymer cross-linked by TO-CNCs. Subsequently, after a critical shear rate of 30 s^{-1}, the network is broken and a sharp decrease can be observed in the viscosity.

Figure 9 attempts to illustrate these two system behaviors.

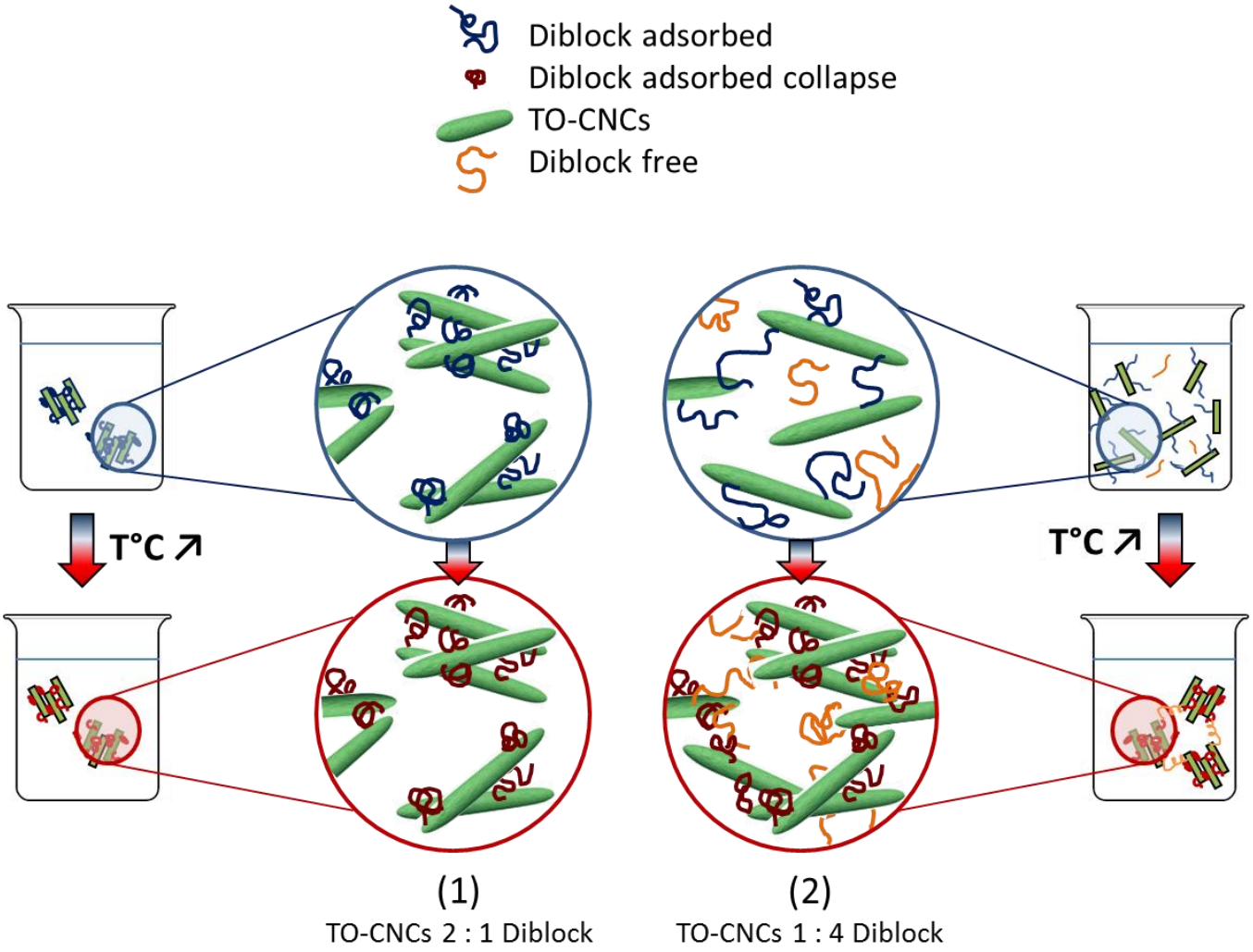

Figure 9. Scheme of the two characteristic behavior identified in this work. (1) TO-CNCs >> Diblock: polymer-mediated aggregated CNCs without thermo-responsive behavior. (2) TO-CNCs << Diblock: individualized particles with polymer chains in excess which allow a thermo-responsive behavior.

Due to the strong adsorption between the TO-CNCs and block copolymer, it is possible to create a thermo-responsive hydrogel with dilute suspensions of nanocrystals. Below the LCST, the system is a "liquid" and above the LCST, it becomes a "gel." While the ratio is very important, the maximum viscosity can also be tuned by increasing the final concentration. Viscosities greater than 3000 Pa·s (at 0.1 s^{-1}) could be obtained at a particular ratio of the TO-CNCs and block copolymer, but a phase separation was observed.

Conclusions

In this study, we examined the thermo-responsive behavior of a hydrogel based on cellulose nanocrystals and a thermo-responsive polymer. A quaternized block copolymer of PDMAEMA-*b*-PDEGMA was adsorbed on TEMPO-oxidized CNCs. QCM-d and MP-SPR measurements indicated fast and irreversible electrostatic adsorption of the block copolymer onto highly anionic TEMPO-oxidized CNC films. Highlighted by SANS measurements, PDMAEMA-b-PDEGMA block copolymers become more hydrophobic and turn into well-defined globules through association of collapse chains upon heating. Adsorbed on the TO-CNC surfaces, block copolymers chains connect CNC bundles and induce the aggregation of TO-CNCs to create dense aggregates when the critical temperature (LCST) is reached. A synergistic effect between the TEMPO-oxidized CNCs and the block copolymer was shown by rheological flow-curve experiments. But, only a high amount of the block copolymer (four times the TO-CNCs mass) in the suspension leads to an appreciable thermo-reversible behavior above the LCST of the polymer when individualized particles CNCs-polymers appear. There occurs a transition from a “liquid” state below the LCST to a “gel” state above the LCST. When the LCST is reached, the polymer on the CNC surfaces attracts its neighboring nanoparticles. Later, non-adsorbed polymers connect with these particle aggregates and form a hydrogel. This promising thermo-responsive functionality on bio-based particles paves the way for the design of injectable hydrogels for surgery or anesthetic medicine.

ACKNOWLEDGEMENT

This work was partially supported by the PolyNat Carnot Institute (Investissements d’Avenir – Grant agreement n°ANR-11-CARN-007-01). This study was possible thanks to the facilities at the TekLiCell platform funded by the Région Rhône-Alpes. We would like to thank Jean-Luc PUTAUX (Univ. Grenoble Alpes, CNRS, CERMAV, FRANCE) for sharing his

expertise in TEM imaging. The authors thank the NanoBio-ICMG platform (Grenoble, FR 2607) for granting access to the electron microscopy facility. Michael S. REID and Heera S. MARWAY are thanked for their expertise in MP-SPR experiments and analysis. The authors acknowledge their SANS contact support, Grégory CHABOUSSANT and Fabrice COUSIN (Laboratoire Léon Brillouin - LLB), for their help during manipulation and in modeling data. Joakim ENGTRÖM and Anna CARLMARK would like to acknowledge the Knut and Alice Wallenberg foundation through the Wallenberg Wood Science Centre (WWSC) for financial support.

SUPPORTING INFORMATION

Figure S1: Conductometric and pH titration for TEMPO oxidized CNC

Figure S2: SASView fitting of TEMPO CNCs with a parallelepiped model.

REFERENCES

(1) Dufresne, A. *Nanocellulose: From Nature to High Performance Tailored Materials*; Walter de Gruyter, 2013.

(2) Abitbol, T.; Rivkin, A.; Cao, Y.; Nevo, Y.; Abraham, E.; Ben-Shalom, T.; Lapidot, S.; Shoseyov, O. Nanocellulose, a Tiny Fiber with Huge Applications. *Curr. Opin. Biotechnol.* **2016**, *39*, 76–88. https://doi.org/10.1016/j.copbio.2016.01.002.

(3) De France, K. J.; Hoare, T.; Cranston, E. D. Review of Hydrogels and Aerogels Containing Nanocellulose. *Chem. Mater.* **2017**, *29* (11), 4609–4631. https://doi.org/10.1021/acs.chemmater.7b00531.

(4) Xu, Y.; Atrens, A. D.; Stokes, J. R. "Liquid, Gel and Soft Glass" Phase Transitions and Rheology of Nanocrystalline Cellulose Suspensions as a Function of Concentration and Salinity. *Soft Matter* **2018**, *14* (10), 1953–1963. https://doi.org/10.1039/C7SM02470C.

(5) Dufresne, A. Nanocellulose: A New Ageless Bionanomaterial. *Mater. Today* **2013**, *16* (6), 220–227. https://doi.org/10.1016/j.mattod.2013.06.004.

(6) Eichhorn, S. J.; Dufresne, A.; Aranguren, M.; Marcovich, N. E.; Capadona, J. R.; Rowan, S. J.; Weder, C.; Thielemans, W.; Roman, M.; Renneckar, S.; et al. Review: Current International Research into Cellulose Nanofibres and Nanocomposites. *J. Mater. Sci.* **2010**, *45* (1), 1–33. https://doi.org/10.1007/s10853-009-3874-0.

(7) Oksman, K.; Mathew, A. P.; Bismarck, A.; Rojas, O.; Sain, M. *Handbook of Green Materials: Processing Technologies, Properties and Applications: Volume 5*; World Scientific, 2014; Vol. 5.

(8) Siqueira, G.; Bras, J.; Dufresne, A. Cellulosic Bionanocomposites: A Review of Preparation, Properties and Applications. *Polymers* **2010**, *2* (4), 728–765. https://doi.org/10.3390/polym2040728.

(9) Camarero Espinosa, S.; Rothen-Rutishauser, B.; Johan Foster, E.; Weder, C. Articular Cartilage: From Formation to Tissue Engineering. *Biomater. Sci.* **2016**, *4* (5), 734–767. https://doi.org/10.1039/C6BM00068A.

(10) Domingues, R. M. A.; Gomes, M. E.; Reis, R. L. The Potential of Cellulose Nanocrystals in Tissue Engineering Strategies. *Biomacromolecules* **2014**, *15* (7), 2327–2346. https://doi.org/10.1021/bm500524s.

(11) Endes, C.; Camarero-Espinosa, S.; Mueller, S.; Foster, E. J.; Petri-Fink, A.; Rothen-Rutishauser, B.; Weder, C.; Clift, M. J. D. A Critical Review of the Current Knowledge Regarding the Biological Impact of Nanocellulose. *J. Nanobiotechnology* **2016**, *14*, 78. https://doi.org/10.1186/s12951-016-0230-9.

(12) Jorfi, M.; Foster, E. J. Recent Advances in Nanocellulose for Biomedical Applications. *J. Appl. Polym. Sci.* **2015**, *132* (14). https://doi.org/10.1002/app.41719.

(13) Klemm, D.; Kramer, F.; Moritz, S.; Lindström, T.; Ankerfors, M.; Gray, D.; Dorris, A. Nanocelluloses: A New Family of Nature-Based Materials. *Angew. Chem. Int. Ed.* **2011**, *50* (24), 5438–5466. https://doi.org/10.1002/anie.201001273.

(14) Lin, N.; Dufresne, A. Nanocellulose in Biomedicine: Current Status and Future Prospect. *Eur. Polym. J.* **2014**, *59*, 302–325.

(15) Naseri, N.; Deepa, B.; Mathew, A. P.; Oksman, K.; Girandon, L. Nanocellulose-Based Interpenetrating Polymer Network (IPN) Hydrogels for Cartilage Applications. *Biomacromolecules* **2016**, *17* (11), 3714–3723. https://doi.org/10.1021/acs.biomac.6b01243.

(16) Gicquel, E.; Martin, C.; Yanez, J. G.; Bras, J. Cellulose Nanocrystals as New Bio-Based Coating Layer for Improving Fiber-Based Mechanical and Barrier Properties. *J. Mater. Sci.* **2017**, *52* (6), 3048–3061. https://doi.org/10.1007/s10853-016-0589-x.
(17) Hoeng, F.; Denneulin, A.; Bras, J. Use of Nanocellulose in Printed Electronics: A Review. *Nanoscale* **2016**, *8* (27), 13131–13154. https://doi.org/10.1039/C6NR03054H.
(18) Li, F.; Biagioni, P.; Bollani, M.; Maccagnan, A.; Piergiovanni, L. Multi-Functional Coating of Cellulose Nanocrystals for Flexible Packaging Applications. *Cellulose* **2013**, *20* (5), 2491–2504. https://doi.org/10.1007/s10570-013-0015-3.
(19) De France, K. J.; Chan, K. J. W.; Cranston, E. D.; Hoare, T. Enhanced Mechanical Properties in Cellulose Nanocrystal–Poly(Oligoethylene Glycol Methacrylate) Injectable Nanocomposite Hydrogels through Control of Physical and Chemical Cross-Linking. *Biomacromolecules* **2016**, *17* (2), 649–660. https://doi.org/10.1021/acs.biomac.5b01598.
(20) Azzam, F.; Siqueira, E.; Fort, S.; Hassaini, R.; Pignon, F.; Travelet, C.; Putaux, J.-L.; Jean, B. Tunable Aggregation and Gelation of Thermoresponsive Suspensions of Polymer-Grafted Cellulose Nanocrystals. *Biomacromolecules* **2016**, *17* (6), 2112–2119. https://doi.org/10.1021/acs.biomac.6b00344.
(21) Schattling, P.; D. Jochum, F.; Theato, P. Multi-Stimuli Responsive Polymers – the All-in-One Talents. *Polym. Chem.* **2014**, *5* (1), 25–36. https://doi.org/10.1039/C3PY00880K.
(22) Way, A. E.; Hsu, L.; Shanmuganathan, K.; Weder, C.; Rowan, S. J. PH-Responsive Cellulose Nanocrystal Gels and Nanocomposites. *ACS Macro Lett.* **2012**, *1* (8), 1001–1006. https://doi.org/10.1021/mz3003006.
(23) Wu, W.; Huang, F.; Pan, S.; Mu, W.; Meng, X.; Yang, H.; Xu, Z.; Ragauskas, A. J.; Deng, Y. Thermo-Responsive and Fluorescent Cellulose Nanocrystals Grafted with Polymer Brushes. *J. Mater. Chem. A* **2015**, *3* (5), 1995–2005. https://doi.org/10.1039/C4TA04761C.
(24) Tripathy, S. K.; Kumar, J.; Nalwa, H. S. *Handbook of Polyelectrolytes and Their Applications: Applications of Polyelectrolytes and Theoretical Models*; American Scientific Publishers, 2002; Vol. 3.
(25) Eyley, S.; Thielemans, W. Surface Modification of Cellulose Nanocrystals. *Nanoscale* **2014**, *6* (14), 7764–7779. https://doi.org/10.1039/c4nr01756k.
(26) J. Eichhorn, S. Cellulose Nanowhiskers: Promising Materials for Advanced Applications. *Soft Matter* **2011**, *7* (2), 303–315. https://doi.org/10.1039/C0SM00142B.
(27) Tang, J.; Sisler, J.; Grishkewich, N.; Tam, K. C. Functionalization of Cellulose Nanocrystals for Advanced Applications. *J. Colloid Interface Sci.* **2017**, *494*, 397–409. https://doi.org/10.1016/j.jcis.2017.01.077.
(28) Habibi, Y. Key Advances in the Chemical Modification of Nanocelluloses. *Chem. Soc. Rev.* **2014**, *43* (5), 1519–1542. https://doi.org/10.1039/C3CS60204D.
(29) Azzam, F.; Heux, L.; Putaux, J.-L.; Jean, B. Preparation By Grafting Onto, Characterization, and Properties of Thermally Responsive Polymer-Decorated Cellulose Nanocrystals. *Biomacromolecules* **2010**, *11* (12), 3652–3659. https://doi.org/10.1021/bm101106c.
(30) Espino-Pérez, E.; Domenek, S.; Belgacem, N.; Sillard, C.; Bras, J. Green Process for Chemical Functionalization of Nanocellulose with Carboxylic Acids. *Biomacromolecules* **2014**, *15* (12), 4551–4560. https://doi.org/10.1021/bm5013458.
(31) Hakalahti, M.; Mautner, A.; Johansson, L.-S.; Hänninen, T.; Setälä, H.; Kontturi, E.; Bismarck, A.; Tammelin, T. Direct Interfacial Modification of Nanocellulose Films for Thermoresponsive Membrane Templates. *ACS Appl. Mater. Interfaces* **2016**, *8* (5), 2923–2927. https://doi.org/10.1021/acsami.5b12300.

(32) Krouit, M.; Bras, J.; Belgacem, M. N. Cellulose Surface Grafting with Polycaprolactone by Heterogeneous Click-Chemistry. *Eur. Polym. J.* **2008**, *44* (12), 4074–4081. https://doi.org/10.1016/j.eurpolymj.2008.09.016.

(33) Vuoriluoto, M.; Orelma, H.; Johansson, L.-S.; Zhu, B.; Poutanen, M.; Walther, A.; Laine, J.; Rojas, O. J. Effect of Molecular Architecture of PDMAEMA–POEGMA Random and Block Copolymers on Their Adsorption on Regenerated and Anionic Nanocelluloses and Evidence of Interfacial Water Expulsion. *J. Phys. Chem. B* **2015**, *119* (49), 15275–15286. https://doi.org/10.1021/acs.jpcb.5b07628.

(34) Yang, H.; Zhu, H.; Hendrix, M. M. R. M.; Lousberg, N. J. H. G. M.; de With, G.; Esteves, A. C. C.; Xin, J. H. Temperature-Triggered Collection and Release of Water from Fogs by a Sponge-Like Cotton Fabric. *Adv. Mater.* **2013**, *25* (8), 1150–1154. https://doi.org/10.1002/adma.201204278.

(35) Zoppe, J. O.; Habibi, Y.; Rojas, O. J.; Venditti, R. A.; Johansson, L.-S.; Efimenko, K.; Österberg, M.; Laine, J. Poly(N-Isopropylacrylamide) Brushes Grafted from Cellulose Nanocrystals via Surface-Initiated Single-Electron Transfer Living Radical Polymerization. *Biomacromolecules* **2010**, *11* (10), 2683–2691. https://doi.org/10.1021/bm100719d.

(36) Chang, C.; Zhang, L. Cellulose-Based Hydrogels: Present Status and Application Prospects. *Carbohydr. Polym.* **2011**, *84* (1), 40–53. https://doi.org/10.1016/j.carbpol.2010.12.023.

(37) Utsel, S.; Malmström, E. E.; Carlmark, A.; Wågberg, L. Thermoresponsive Nanocomposites from Multilayers of Nanofibrillated Cellulose and Specially Designed N-Isopropylacrylamide Based Polymers. *Soft Matter* **2010**, *6* (2), 342–352. https://doi.org/10.1039/B910481J.

(38) Ingverud, T.; Larsson, E.; Hemmer, G.; Rojas, R.; Malkoch, M.; Carlmark, A. High Water-Content Thermoresponsive Hydrogels via Electrostatic Macrocrosslinking of Cellulose Nanofibrils. *J. Polym. Sci. Part Polym. Chem.* **2016**, *54* (21), 3415–3424. https://doi.org/10.1002/pola.28225.

(39) Larsson, E.; Sanchez, C. C.; Porsch, C.; Karabulut, E.; Wågberg, L.; Carlmark, A. Thermo-Responsive Nanofibrillated Cellulose by Polyelectrolyte Adsorption. *Eur. Polym. J.* **2013**, *49* (9), 2689–2696. https://doi.org/10.1016/j.eurpolymj.2013.05.023.

(40) Masci, G.; Ladogana, R. D.; Cametti, C. Assemblies of Thermoresponsive Diblock Copolymers: Micelle and Vesicle Formation Investigated by Means of Dielectric Relaxation Spectroscopy. *J. Phys. Chem. B* **2012**, *116* (7), 2121–2130. https://doi.org/10.1021/jp212065c.

(41) Bercea, M.; Navard, P. Shear Dynamics of Aqueous Suspensions of Cellulose Whiskers. *Macromolecules* **2000**, *33* (16), 6011–6016. https://doi.org/10.1021/ma000417p.

(42) Liu, D.; Chen, X.; Yue, Y.; Chen, M.; Wu, Q. Structure and Rheology of Nanocrystalline Cellulose. *Carbohydr. Polym.* **2011**, *84* (1), 316–322. https://doi.org/10.1016/j.carbpol.2010.11.039.

(43) Liu, H.; Wang, D.; Song, Z.; Shang, S. Preparation of Silver Nanoparticles on Cellulose Nanocrystals and the Application in Electrochemical Detection of DNA Hybridization. *Cellulose* **2011**, *18* (1), 67–74. https://doi.org/10.1007/s10570-010-9464-0.

(44) Lu, A.; Hemraz, U.; Khalili, Z.; Boluk, Y. Unique Viscoelastic Behaviors of Colloidal Nanocrystalline Cellulose Aqueous Suspensions. *Cellulose* **2014**, *21* (3), 1239–1250. https://doi.org/10.1007/s10570-014-0173-y.

(45) Shafiei-Sabet, S.; Hamad, W. Y.; Hatzikiriakos, S. G. Rheology of Nanocrystalline Cellulose Aqueous Suspensions. *Langmuir ACS J. Surf. Colloids* **2012**, *28* (49), 17124–17133. https://doi.org/10.1021/la303380v.

(46) Shafiei-Sabet, S.; Hamad, W. Y.; Hatzikiriakos, S. G. Ionic Strength Effects on the Microstructure and Shear Rheology of Cellulose Nanocrystal Suspensions. *Cellulose* **2014**, *21* (5), 3347–3359. https://doi.org/10.1007/s10570-014-0407-z.

(47) Ureña-Benavides, E. E.; Ao, G.; Davis, V. A.; Kitchens, C. L. Rheology and Phase Behavior of Lyotropic Cellulose Nanocrystal Suspensions. *Macromolecules* **2011**, *44* (22), 8990–8998. https://doi.org/10.1021/ma201649f.

(48) Xu, H.-N.; Tang, Y.-Y.; Ouyang, X.-K. Shear-Induced Breakup of Cellulose Nanocrystal Aggregates. *Langmuir* **2017**, *33* (1), 235–242. https://doi.org/10.1021/acs.langmuir.6b03807.

(49) Xu, Y.; Atrens, A. D.; Stokes, J. R. Rheology and Microstructure of Aqueous Suspensions of Nanocrystalline Cellulose Rods. *J. Colloid Interface Sci.* **2017**, *496*, 130–140. https://doi.org/10.1016/j.jcis.2017.02.020.

(50) Sanna, R.; Fortunati, E.; Alzari, V.; Nuvoli, D.; Terenzi, A.; Casula, M. F.; Kenny, J. M.; Mariani, A. Poly(N-Vinylcaprolactam) Nanocomposites Containing Nanocrystalline Cellulose: A Green Approach to Thermoresponsive Hydrogels. *Cellulose* **2013**, *20* (5), 2393–2402. https://doi.org/10.1007/s10570-013-9988-1.

(51) Zoppe, J. O.; Venditti, R. A.; Rojas, O. J. Pickering Emulsions Stabilized by Cellulose Nanocrystals Grafted with Thermo-Responsive Polymer Brushes. *J. Colloid Interface Sci.* **2012**, *369* (1), 202–209. https://doi.org/10.1016/j.jcis.2011.12.011.

(52) Zhou, C.; Wu, Q.; Zhang, Q. Dynamic Rheology Studies of in Situ Polymerization Process of Polyacrylamide–cellulose Nanocrystal Composite Hydrogels. *Colloid Polym. Sci.* **2011**, *289* (3), 247–255. https://doi.org/10.1007/s00396-010-2342-3.

(53) Hemraz, U. D.; Lu, A.; Sunasee, R.; Boluk, Y. Structure of Poly(N-Isopropylacrylamide) Brushes and Steric Stability of Their Grafted Cellulose Nanocrystal Dispersions. *J. Colloid Interface Sci.* **2014**, *430*, 157–165. https://doi.org/10.1016/j.jcis.2014.05.011.

(54) Habibi, Y.; Chanzy, H.; Vignon, M. R. TEMPO-Mediated Surface Oxidation of Cellulose Whiskers. *Cellulose* **2006**, *13* (6), 679–687. https://doi.org/10.1007/s10570-006-9075-y.

(55) Horn, D. Optisches Zweistrahlverfahren zur Bestimmung von Polyelektrolyten in Wasser und zur Messung der Polymeradsorption an Grenzflächen. *SpringerLink* **1978**, 251–264. https://doi.org/10.1007/978-3-642-93664-7_28.

(56) Foster, E. J.; Moon, R. J.; Agarwal, U. P.; Bortner, M. J.; Bras, J.; Camarero-Espinosa, S.; Chan, K. J.; Clift, M. J.; Cranston, E. D.; Eichhorn, S. J. Current Characterization Methods for Cellulose Nanomaterials. *Chem. Soc. Rev.* **2018**.

(57) Rodahl, M.; Höök, F.; Krozer, A.; Brzezinski, P.; Kasemo, B. Quartz Crystal Microbalance Setup for Frequency and *Q* -factor Measurements in Gaseous and Liquid Environments. *Rev. Sci. Instrum.* **1995**, *66* (7), 3924–3930. https://doi.org/10.1063/1.1145396.

(58) Sauerbrey, G. Z. Use of Quartz Vibration for Weighing Thin Films on a Microbalance. *J Phys.* **1959**, *155*, 206–212.

(59) Irwin, E. F.; Ho, J. E.; Kane, S. R.; Healy, K. E. Analysis of Interpenetrating Polymer Networks via Quartz Crystal Microbalance with Dissipation Monitoring. *Langmuir* **2005**, *21* (12), 5529–5536. https://doi.org/10.1021/la0470737.

(60) Voinova, M. V.; Rodahl, M.; Jonson, M.; Kasemo, B. Viscoelastic Acoustic Response of Layered Polymer Films at Fluid-Solid Interfaces: Continuum Mechanics Approach. *Phys. Scr.* **1999**, *59* (5), 391–396.

(61) Aulin, C.; Varga, I.; Claesson, P. M.; Wågberg, L.; Lindström, T. Buildup of Polyelectrolyte Multilayers of Polyethyleneimine and Microfibrillated Cellulose Studied by in Situ Dual-Polarization Interferometry and Quartz Crystal Microbalance

with Dissipation. *Langmuir* **2008**, *24* (6), 2509–2518. https://doi.org/10.1021/la7032884.
(62) Karabulut, E.; Pettersson, T.; Ankerfors, M.; Wågberg, L. Adhesive Layer-by-Layer Films of Carboxymethylated Cellulose Nanofibril–Dopamine Covalent Bioconjugates Inspired by Marine Mussel Threads. *ACS Nano* **2012**, *6* (6), 4731–4739. https://doi.org/10.1021/nn204620j.
(63) Krivosheeva, O.; Sababi, M.; Dedinaite, A.; Claesson, P. M. Nanostructured Composite Layers of Mussel Adhesive Protein and Ceria Nanoparticles. *Langmuir* **2013**, *29* (30), 9551–9561. https://doi.org/10.1021/la401693x.
(64) Reid, M.; Villalobos, M.; Cranston, E. Cellulose Nanocrystal Interactions Probed by Thin Film Swelling to Predict Dispersibility. *Nanoscale* **2016**, *8* (24), 12247–12257. https://doi.org/10.1039/C6NR01737A.
(65) Liang, H.; Miranto, H.; Granqvist, N.; Sadowski, J. W.; Viitala, T.; Wang, B.; Yliperttula, M. Surface Plasmon Resonance Instrument as a Refractometer for Liquids and Ultrathin Films. *Sens. Actuators B Chem.* **2010**, *149* (1), 212–220.
(66) Schasfoort, R. B. M.; Tudos, A. J. *Handbook of Surface Plasmon Reso-NanceRoyal Society of Chemistry*; London, 2008.
(67) Jung, L. S.; Campbell, C. T.; Chinowsky, T. M.; Mar, M. N.; Yee, S. S. Quantitative Interpretation of the Response of Surface Plasmon Resonance Sensors to Adsorbed Films. *Langmuir* **1998**, *14* (19), 5636–5648.
(68) Lee, B. S.; Chi, Y. S.; Lee, K.-B.; Kim, Y.-G.; Choi, I. S. Functionalization of Poly (Oligo (Ethylene Glycol) Methacrylate) Films on Gold and Si/SiO2 for Immobilization of Proteins and Cells: SPR and QCM Studies. *Biomacromolecules* **2007**, *8* (12), 3922–3929.
(69) Campbell, C. T.; Kim, G. SPR Microscopy and Its Applications to High-Throughput Analyses of Biomolecular Binding Events and Their Kinetics. *Biomaterials* **2007**, *28* (15), 2380–2392.
(70) Feng, W.; Zhu, S.; Ishihara, K.; Brash, J. L. Protein Resistant Surfaces: Comparison of Acrylate Graft Polymers Bearing Oligo-Ethylene Oxide and Phosphorylcholine Side Chains. *Biointerphases* **2006**, *1* (1), 50–60.
(71) Brûlet, A.; Lairez, D.; Lapp, A.; Cotton, J.-P. Improvement of Data Treatment in Small-Angle Neutron Scattering. *J. Appl. Crystallogr.* **2007**, *40* (1), 165–177.
(72) Habibi, Y.; Lucia, L. A.; Rojas, O. J. Cellulose Nanocrystals: Chemistry, Self-Assembly, and Applications. *Chem. Rev.* **2010**, *110* (6), 3479–3500. https://doi.org/10.1021/cr900339w.
(73) Hoogeveen, N. G.; Stuart, M. A. C.; Fleer, G. J. Polyelectrolyte Adsorption on Oxides: II. Reversibility and Exchange. *J. Colloid Interface Sci.* **1996**, *182* (1), 146–157.
(74) Araki, J.; Wada, M.; Kuga, S. Steric Stabilization of a Cellulose Microcrystal Suspension by Poly(Ethylene Glycol) Grafting. *Langmuir* **2000**, *17* (1), 21–27. https://doi.org/10.1021/la001070m.
(75) Grishkewich, N.; Akhlaghi, S. P.; Zhaoling, Y.; Berry, R.; Tam, K. C. Cellulose Nanocrystal-Poly(Oligo(Ethylene Glycol) Methacrylate) Brushes with Tunable LCSTs. *Carbohydr. Polym.* **2016**, *144*, 215–222. https://doi.org/10.1016/j.carbpol.2016.02.044.
(76) Reid, M. S.; Villalobos, M.; Cranston, E. D. The Role of Hydrogen Bonding in Non-Ionic Polymer Adsorption to Cellulose Nanocrystals and Silica Colloids. *Curr. Opin. Colloid Interface Sci.* **2017**, *29*, 76–82. https://doi.org/10.1016/j.cocis.2017.03.005.
(77) Mao, Y.; Liu, K.; Zhan, C.; Geng, L.; Chu, B.; Hsiao, B. S. Characterization of Nanocellulose Using Small-Angle Neutron, X-Ray, and Dynamic Light Scattering

Techniques. *J. Phys. Chem. B* **2017**, *121* (6), 1340–1351. https://doi.org/10.1021/acs.jpcb.6b11425.

(78) Ewart, R. H.; Roe, C. P.; Debye, P.; McCartney, J. R. The Determination of Polymeric Molecular Weights by Light Scattering in Solvent-Precipitant Systems. *J. Chem. Phys.* **1946**, *14* (11), 687–695. https://doi.org/10.1063/1.1724085.

(79) Wu, Q.; Meng, Y.; Wang, S.; Li, Y.; Fu, S.; Ma, L.; Harper, D. Rheological Behavior of Cellulose Nanocrystal Suspension: Influence of Concentration and Aspect Ratio. *J. Appl. Polym. Sci.* **2014**, *131* (15), 40525. https://doi.org/10.1002/app.40525.

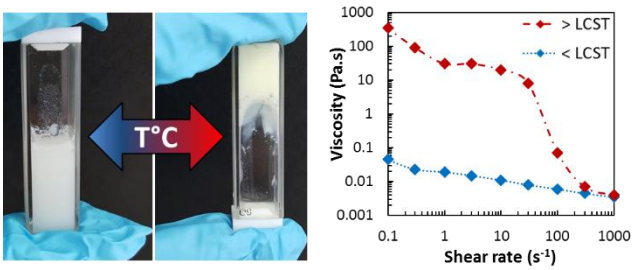

Table of content Graphic